



## Prediction of interfacial shear stress and pressure drop in vertical two-phase annular flow

Huacheng Zhang<sup>a</sup>, Yutaro Umebara<sup>a</sup>, Hiroyuki Yoshida<sup>b</sup>, Shoji Mori<sup>a,\*</sup>

<sup>a</sup> Department of Mechanical Engineering, Graduate School of Engineering, Kyushu University, 744 Motooka, Nishi-ku, Fukuoka 819-0395, Japan

<sup>b</sup> Japan Atomic Energy Agency, 2-4 Shirakata, Tokai-mura, Naka-gun, Ibaraki 319-1195, Japan



### ARTICLE INFO

#### Keywords:

Annular flow  
Disturbance wave  
Interfacial shear stress  
Pressure drop

### ABSTRACT

The interfacial shear stress and pressure drop of an upward vertical annular flow of nitrogen–water, HFC134a–water, and nitrogen–95 % ethanol solution were comprehensively investigated considering the effect of the liquid–gas density ratio and surface tension. A direct link between the disturbance wave height and equivalent sand-grain roughness was noted through the analogy with the famous Moody chart for single-phase turbulent flows. A predictive model of the interfacial friction factor was developed based on this finding. To predict the pressure drop of the annular flow, a new model with good predictive performance for annular flows of various working fluids including steam–water under boiling water reactor operating condition (286 °C and 7 MPa) was proposed.

### 1. Introduction

Annular flow is a two-phase flow regime encountered in different industries, such as nuclear reactors, refrigeration systems, and gas transportation. This consists of a continuously flowing gas core, liquid film attached to the tube wall, and intermittent disturbance waves at the gas–liquid interface. In several industrial applications, especially energy facilities, the accurate prediction of the pressure drop of two-phase flow systems is critical in increasing the energy conversion efficiency.

Accompanied by the wavy structure of the gas–liquid interface, the gas at the core flows upward with a larger frictional pressure drop than that in a smooth wall tube for a single-phase flow owing to the higher interfacial shear stress,  $\tau_i$ , induced by the roughened interface. Considering the critical contribution of the interfacial shear stress on the pressure drop in two-phase annular flows, interference with the force balances of both the gas core and liquid film coupled with the liquid film characteristics in the accurate prediction of the interfacial shear stress has garnered considerable attention from numerous researchers.

Conventionally, interfacial shear stress is expressed in an equation involving the gas density, gas velocity, and interfacial friction factor, which is denoted by  $C_{fi}$ . Wallis [1] derived the correlation of the interfacial friction factor considering the liquid film as the rough wall in a single-phase flow. Consequently, various correlations of the interfacial friction factor have been proposed. To the best of the authors'

knowledge, these correlations can be roughly divided into four types based on their derivation method.

The first type of the  $C_{fi}$  correlations is the Wallis-type correlation, which is mostly arithmetic modifications of the Wallis correlation. For example, Moeck raised the exponent of the dimensionless average film thickness and altered the other coefficients [2]. Fukano and Furukawa introduced a liquid kinetic viscosity to account for the effect of the change in the viscosity of the working fluid [3]. Fore et al. added the gas Reynolds number to the Wallis correlation to better predict  $C_{fi}$  over a wide range of gas Reynolds numbers and liquid film thicknesses [4]. Ju et al. derived the  $C_{fi}$  correlation by introducing the Weber numbers and viscosity number, which are related to the dimensionless average film thickness, into the Wallis correlation [5].

The second type of  $C_{fi}$  correlations relate the interfacial friction factor to the sand-grain roughness of a turbulent single-phase flow in rough pipes. Oliemans et al. [6] obtained the correlation for the interfacial roughness based on the gas Weber number and combined it with the phenomenological Colebrook equation [7], which expresses the Darcy friction factor as a function of the Reynolds number and wall roughness, to predict  $C_{fi}$ . Belt et al. determined the relationship between the average film thickness and equivalent sand-grain roughness from the Churchill equation [8], which is a famous approximation of the Colebrook equation, and derived the empirical correlation for  $C_{fi}$  [9].

The third type of  $C_{fi}$  correlations can be treated as modifications of the Wallis equation using a computed single-phase gas friction factor for

\* Corresponding author.

E-mail address: [morisho@mech.kyushu-u.ac.jp](mailto:morisho@mech.kyushu-u.ac.jp) (S. Mori).

Nomenclature	
$C$	Chisholm parameter (-)
$C_f$	friction factor (-)
$D$	tube diameter (m)
$G$	mass flux ( $\text{kg}/\text{m}^2 \cdot \text{s}$ )
$E$	entrainment rate (-)
$g$	acceleration due to gravity ( $\text{m}/\text{s}^2$ )
$H$	wave height (m)
$j$	superficial velocity (m/s)
$k_s$	equivalent sand-grain roughness (m)
$N_\mu$	viscosity number (-)
$P$	pressure (Pa)
$R_D$	deposition rate ( $\text{kg}/\text{m}^2 \cdot \text{s}$ )
$Re$	Reynolds number (-)
$t_F$	film thickness (m)
$u$	velocity (m/s)
$We$	Weber number (-)
$X$	Lockhart–Martinelli parameter (-)
$x$	vapor quality (-)
$z$	axial position (m)
Greek symbols	
$\alpha_d$	droplet volume fraction (-)
$\mu$	dynamic viscosity (Pa·s)
$\rho$	density ( $\text{kg}/\text{m}^3$ )
$\sigma$	surface tension (N/m)
$\tau$	shear stress (Pa)
$\Phi$	two-phase frictional multiplier (-)
Subscripts	
$ave$	average value
$c$	core
$G$	gas phase
$i$	interface
$L$	liquid phase
$TP$	Two-phase
$w$	disturbance wave

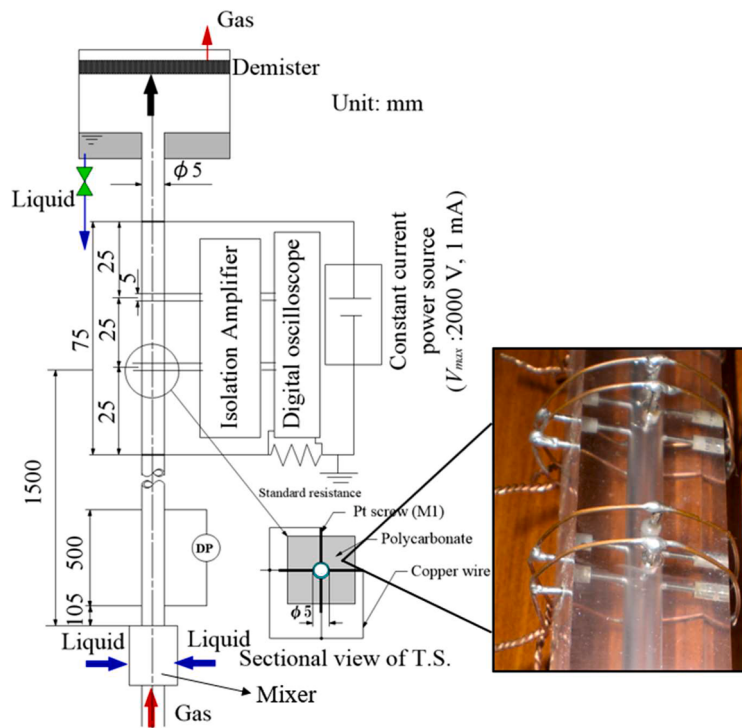


Fig. 1. Schematic of the test section.

Table 1

Summary of the properties of the working fluids.

System	Pressure [MPa]	Temperature [ $^\circ\text{C}$ ]	$\rho_G$ [ $\text{kg}/\text{m}^3$ ]	$\rho_L$ [ $\text{kg}/\text{m}^3$ ]	$\sigma$ [mN/m]	$\mu_G$ [ $\mu\text{Pa}\cdot\text{s}$ ]	$\mu_L$ [ $\mu\text{Pa}\cdot\text{s}$ ]	$\rho_L / \rho_G$ [-]
Nitrogen–Water	0.2	25	2.3	997.0	67.4	17.7	850.0	434
	0.4	25	4.5	997.0	67.4	17.7	850.0	222
HFC134a–Water	0.7	40	31.5	992.0	59.0	12.3	570.0	32
Nitrogen–95 % Ethanol	0.2	25	2.3	850.0	30.7	17.7	1420.0	370

a smooth wall tube,  $C_{fs}$ , that replace the constant of 0.005 in the Wallis equation, as represented by Henstock [10], Asali [11], Hajiloo [12], and Aliyu [13,14]. Finally, the fourth type of  $C_{fi}$  correlations is based on the

dimensional analysis of the experimental data derived by Cioncolini et al. [15].

Although the interfacial shear stress of annular flows has been

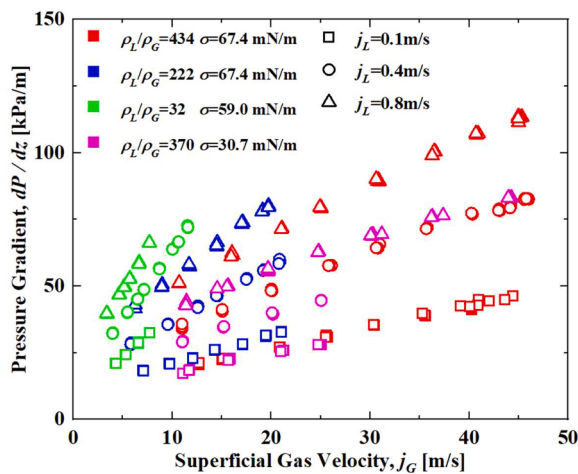


Fig. 2. Measured pressure gradient over 0.5 m.

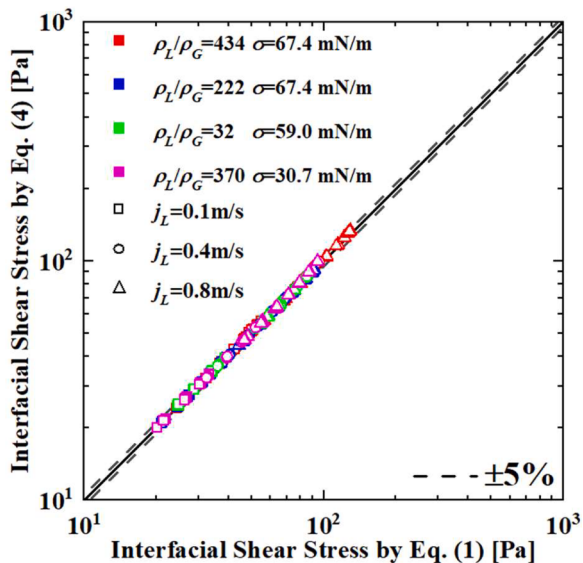


Fig. 3. Comparison of the interfacial shear stress calculated by Eqs. (1) and (4).

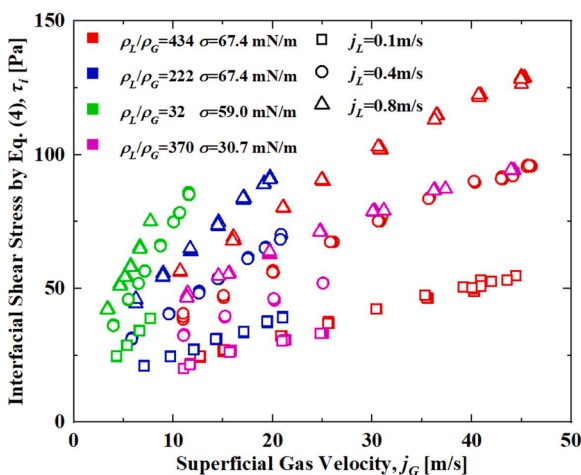


Fig. 4. Interfacial shear stress calculated by Eq. (4).

investigated extensively [15–18], most experiments available in the literature were conducted using air and water under nearly atmospheric pressure. As such, the variety of fluid properties in existing studies is limited. The authors have previously reported the effect of density ratio and surface tension on the liquid film thickness and disturbance wave height [19], and velocity, longitudinal size, and frequency of disturbance waves [20]. In this work, the effect of density ratio and surface tension on the interfacial shear stress was experimentally studied using nitrogen gas, HFC134a gas, water, and 95 % (v/v) aqueous ethanol solution as working fluids under the pressure of 0.2–0.7 MPa in a 5.0 mm (inner diameter) tube. New models are proposed for predicting the interfacial shear stress and pressure drop for vertical upward annular flow.

## 2. Experimental apparatus and procedures

The main details of the experimental facility for the annular flow measurement are introduced in our previous study [19,20]. The experimental facility was constructed using a nonconductive polycarbonate resin test section with an inner diameter,  $D$ , of 5.0 mm. As shown in Fig. 1, the working liquid and gas were mixed in a mixer at the inlet of the test section and flowed upward to the test section. The mixer is made of a porous tube with an average pore diameter of 120  $\mu\text{m}$  and an inner diameter of 5 mm which is almost equal to that of the test section. The liquid is supplied to the test section through the porous wall, whereas the gas is injected from the bottom of the mixer unit directly into the center of the test section. For the annular flow, this injection method using a porous tube can minimize the entrance effect on the development of the flow [21]. After the test section, the two-phase flow enters the separator along the tube, which extends from the test section to the interior of the separator and is above the liquid level to avoid the unstable flow downstream of the test section.

Two sets of sensors were installed in the test section to measure the electrical conductance of the liquid film at two different locations. Each sensor was composed of two flush-mounted conductance probes used to measure the voltage difference between them. The axial distance between the two conductance probes in each sensor was 5.0 mm and the axial distance between two sensors was 25.0 mm. The distance from the inlet of the test section to the first sensor was 1500 mm. A developing length ( $L/D = 300$ ) was achieved to ensure that the measurements correspond to the fully developed equilibrium annular flow, which is in accordance with the correlation proposed by Kataoka and Ishii [22]. A Kyowa PD-A differential pressure transducer was installed to measure the differential pressure at 0.5–0.105 m downstream the inlet of the test section. The estimated uncertainty of the differential pressure measurement was 10 %.

The electric current of the main circuit was fixed at 1.0 mA. The measurements were carried out with a standard electric resistance of 1  $\text{k}\Omega$ . The time-varying voltage output from the sensors and electric resistance were recorded simultaneously by a digital oscilloscope at a sampling frequency of 5 kHz over the length of 10,000 data points (2 s). From the recorded voltage and current output, the time trace of the liquid film thickness can be obtained similar to that in our previous work. The calibration of sensors has been performed before and after experiments and the error for measuring liquid film thickness is within ca.  $\pm 5$  % with film thickness ranging from 0.1 to 0.5 mm [19]. In current experiments, the average film thickness ranges from ca. 0.06 mm to 0.36 mm.

Table 1 summarizes the experimental conditions in this study, which were the same as those in our previous research [19,20]. The properties of the working liquid and gas are listed. Gas density, liquid density, surface tension, gas viscosity, and liquid viscosity are denoted as  $\rho_G$ ,  $\rho_L$ ,  $\sigma$ ,  $\mu_G$ , and  $\mu_L$ , respectively. The density of the working liquid was obtained with an electronic scale and measuring cylinder. The dynamic viscosity and surface tension of the working liquid was measured before and after each experiment by an A&D SV-10 viscometer with an

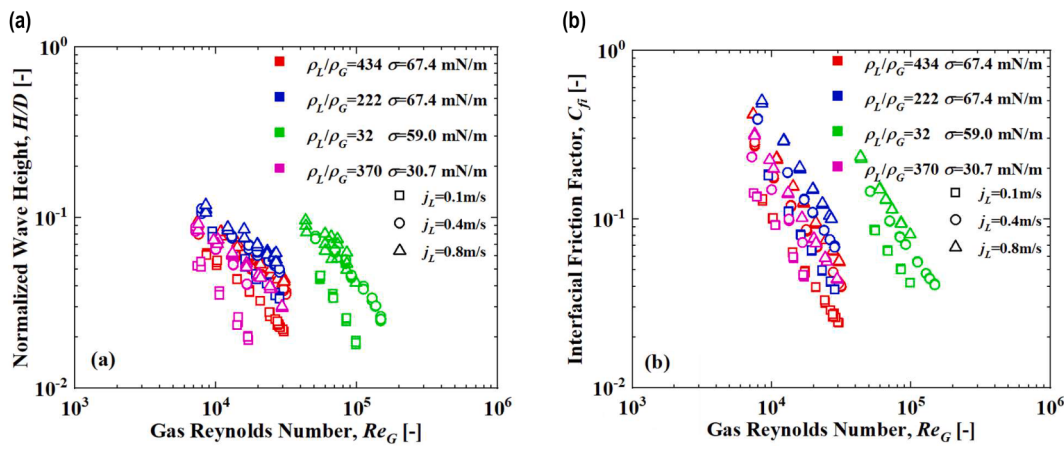
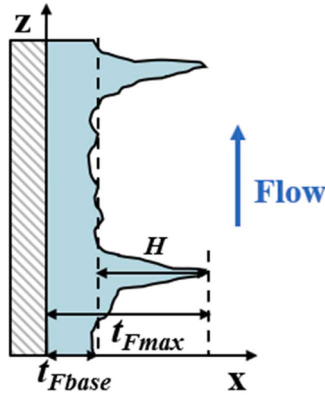
Fig. 5. Comparison between  $Re_G$  and (a)  $H/D$  and (b)  $C_{fi}$ .

Fig. 6. Schematic of the disturbance wave characteristics.

accuracy of 5 % and a Rhesca 5200tn tester with an accuracy of 9 %. The density and dynamic viscosity of the working gas were obtained from literature [23]. Nitrogen gas under 0.2 and 0.4 MPa and HFC134a gas under 0.7 MPa were used as working gasses. The superficial liquid velocity,  $j_L$ , at the test section was set at 0.1, 0.4, and 0.8 m/s for each pressure condition. In current experiments, a range of liquid Reynolds number from ca. 320 to 7000 and gas Reynolds number from ca. 7100 to 147,000 were covered while the liquid Weber number ranges from ca. 0.7 to 60 and gas Weber number ranges from ca. 15 to 980. All the flows

in the current experiments were classified as annular flow, as indicated by the flow maps of Hewitt and Roberts [24] and Mishima and Ishii [25]. Additional details on the experimental facility, flow regime, film thickness acquisition, and data processing are provided in our previous work [19,20].

### 3. Results and discussion

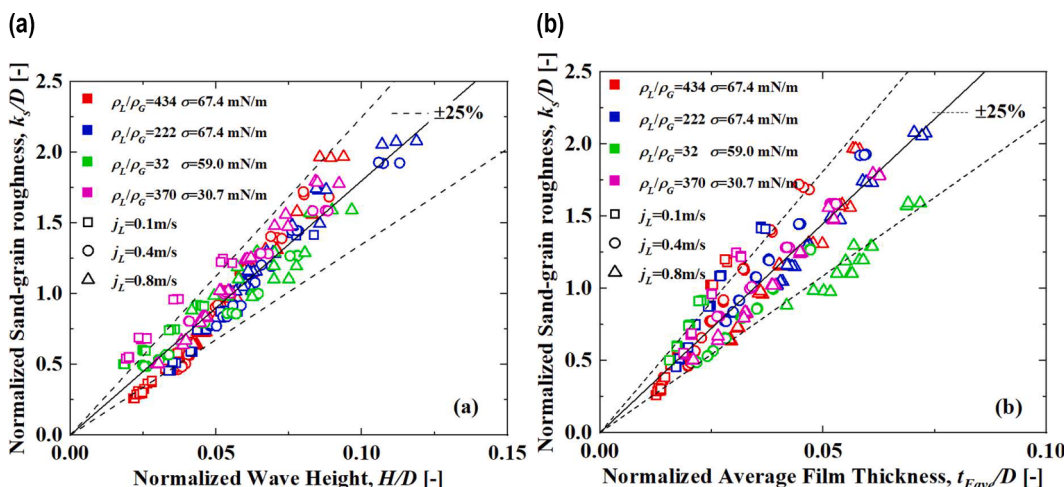
#### 3.1. Pressure gradient and interfacial shear stress

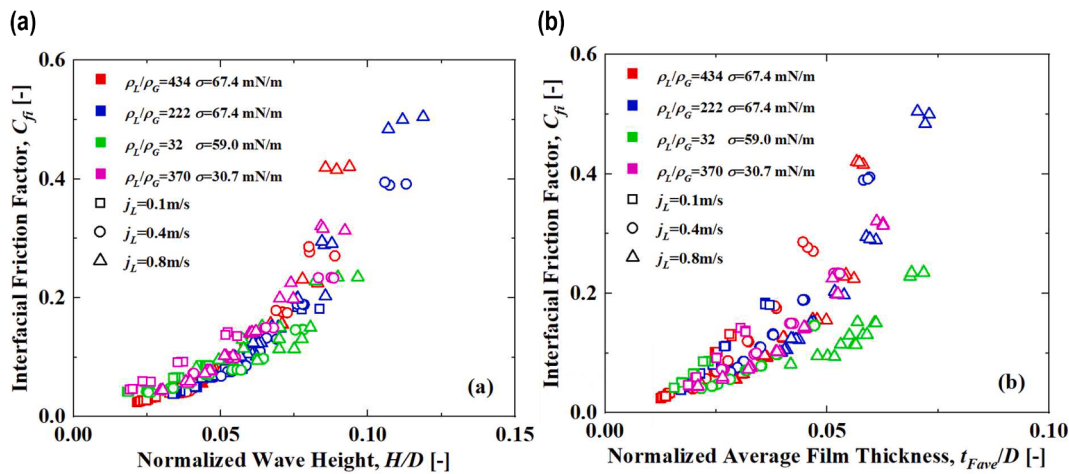
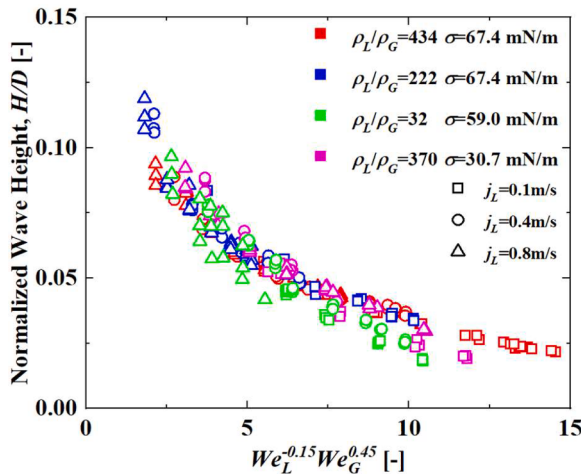
The measured average pressure gradient,  $dP/dz$ , over 0.5 m is presented in Fig. 2. The pressure gradient increases with the increase in the superficial gas velocity,  $j_G$ , and decrease in the density ratio. Moreover, the pressure gradient tends to decrease as the surface tension decreases when  $j_L$  is 0.4 and 0.8 m/s.

Conventionally, for the equilibrium annular flow, the interfacial shear stress can be expressed as [4,5,9,26,27]:

$$\tau_i = -\frac{D - 2t_{Fave}}{4} \left[ \frac{dP}{dz} \left( 1 - \frac{\rho_c j_G^2}{P} \right) + \rho_c g \right] - R_D(u_D - u_E). \quad (1)$$

where  $\frac{dP}{dz}$  (Pa/m) is the pressure gradient,  $t_{Fave}$  (m) is the average film thickness,  $\rho_c$  ( $\text{kg}/\text{m}^3$ ) is the core mixture density,  $P$  (Pa) is the system pressure,  $R_D$  ( $\text{kg}/(\text{m}^2 \text{s})$ ) is the deposition rate,  $u_D$  (m/s) is the mean axial velocity of the depositing drops, and  $u_E$  (m/s) is the mean axial velocity of the entraining drops.  $\rho_c$  can be expressed using the droplet volume fraction inside gas core  $\alpha_d$  and entrainment rate  $E$  from the model of

Fig. 7. Comparison between  $k_s/D$  and (a)  $H/D$ ; (b)  $t_{Fave}/D$ .

Fig. 8. Comparison between  $C_{fi}$  and (a)  $H/D$ ; (b)  $t_{Fave}/D$ .Fig. 9. Comparison between  $H/D$  and  $We_L^{-0.15}We_G^{0.45}$ .

Sawant [28]:

$$\rho_c = (1 - \alpha_d)\rho_G + \alpha_d\rho_L, \quad (2)$$

$$\alpha_d = \frac{Ej_L}{Ej_L + j_G}. \quad (3)$$

However, considering that the maximum entrainment rate in the current experiments is less than 0.05 and the difference between  $\rho_c$  and  $\rho_G$  is less than 10 %,  $\rho_c \approx \rho_G$  was adopted in this study, which has also been adopted by Ju et al. [5] to avoid additional errors.  $R_D$  was estimated using the correlation of Ishii and Mishima [29], as suggested by

Schubring et al. [26]. For simplicity,  $u_E$  and  $u_D$  were estimated by the disturbance wave velocity and actual gas velocity, which is consistent with previous studies [9,26]. Considering the relatively low gas flow rate and small entrainment and deposition rates in current experiments, the frictional pressure drop is expected to be the largest contributor to the total pressure drop. Therefore, as suggested by previous studies [3, 27], the interfacial shear stress is expressed as:

$$\tau_i = -\frac{D - 2t_{Fave}}{4} \frac{dP}{dz}. \quad (4)$$

The interfacial shear stress calculated using Eqs. (1) and (4) were compared, as shown in Fig. 3, whereby the maximum deviation between them is 5.7 %. For simplicity,  $\tau_i$  was computed by Eq. (4) in this work.

The  $\tau_i$  calculated from Eq. (4) was plotted against  $j_G$ , as shown in the Fig. 4, resulting in a similar tendency as that with the  $dP/dz$ . In particular,  $\tau_i$  increases with the increase in  $j_G$  and decrease in density ratio.

**Table 3**  
Previous models of the interfacial friction factor.

Refs.	Correlation
Moeck [2]	$C_{fi} = 0.005 \left( 1 + 1090 \left( \frac{t_{Fave}}{D} \right)^{1.42} \right)$
Fore et al. [4]	$C_{fi} = 0.005 \left[ 1 + 300 \left( 1, + \frac{1,750,0}{Re_G} \right) \frac{t_{Fave}}{D} - 0.0015 \right]$
Ju et al. [5]	$C_{fi} = 0.0028 + 4.28 We_L^{0.28} We_G^{-0.53} N_{pl}^{0.25}$
Belt et al. [9]	$C_{fi} = 2 \left( 1.158 \frac{t_{Fave}}{D} + 0.0003413 \right)$
Henstock and Hanratty [10]	$C_{fi} = C_{fs} (1 + 1400F), C_{fs} = \frac{0.046}{Re_G^{0.2}}, F = \frac{1}{\sqrt{2} Re_G^{0.4} Re_G^{0.5}} \frac{\mu_L}{\mu_G} \frac{\rho_G^{0.5}}{\rho_L^{0.5}}$ for $Re_L < 1000, Re_G < 1000; F = \frac{0.0379 Re_L^{0.9}}{Re_G^{0.9}} \frac{\mu_L}{\mu_G} \frac{\rho_G^{0.5}}{\rho_L^{0.5}}$ , for $Re_L > 1000, Re_G > 1000$

**Table 2**  
Summary of the experimental conditions of the employed databases.

Reference	$D$ [mm]	$j_L$ [m/s]	$j_G$ [m/s]	Corresponding data range	$\rho_L/\rho_G$ [-]	$\sigma$ [mN/m]
Current experiments	5.0	0.1, 0.4, and 0.8	3–45	Nitrogen–Water (0.2 and 0.4 MPa), nitrogen–95 % aqueous ethanol solution (0.2 MPa), and HFC134a–water (0.7 MPa)	32–434	30.7–67.4
Sawant et al. [34]	9.4	0.05, 0.1, 0.15, 0.3, and 0.54	3–111	Air–Water 0.12, 0.4, and 0.58 MPa	147–712	72.3
Wang et al. [27]	25.4	0.06, 0.15, 0.3, and 0.5	10–27	Air–water near atmospheric pressure	874	73.0
Fukano and Furukawa [3]	26	0.04, 0.06, and 0.1	10–50	Air–Water and 45 wt % Glycerol solution 0.13–0.117 MPa	786–876	72.0 and 65.0
Würtz [35]	10 and 20	0.06–2.49	3–22	Steam–Water 7 MPa	20	17.7

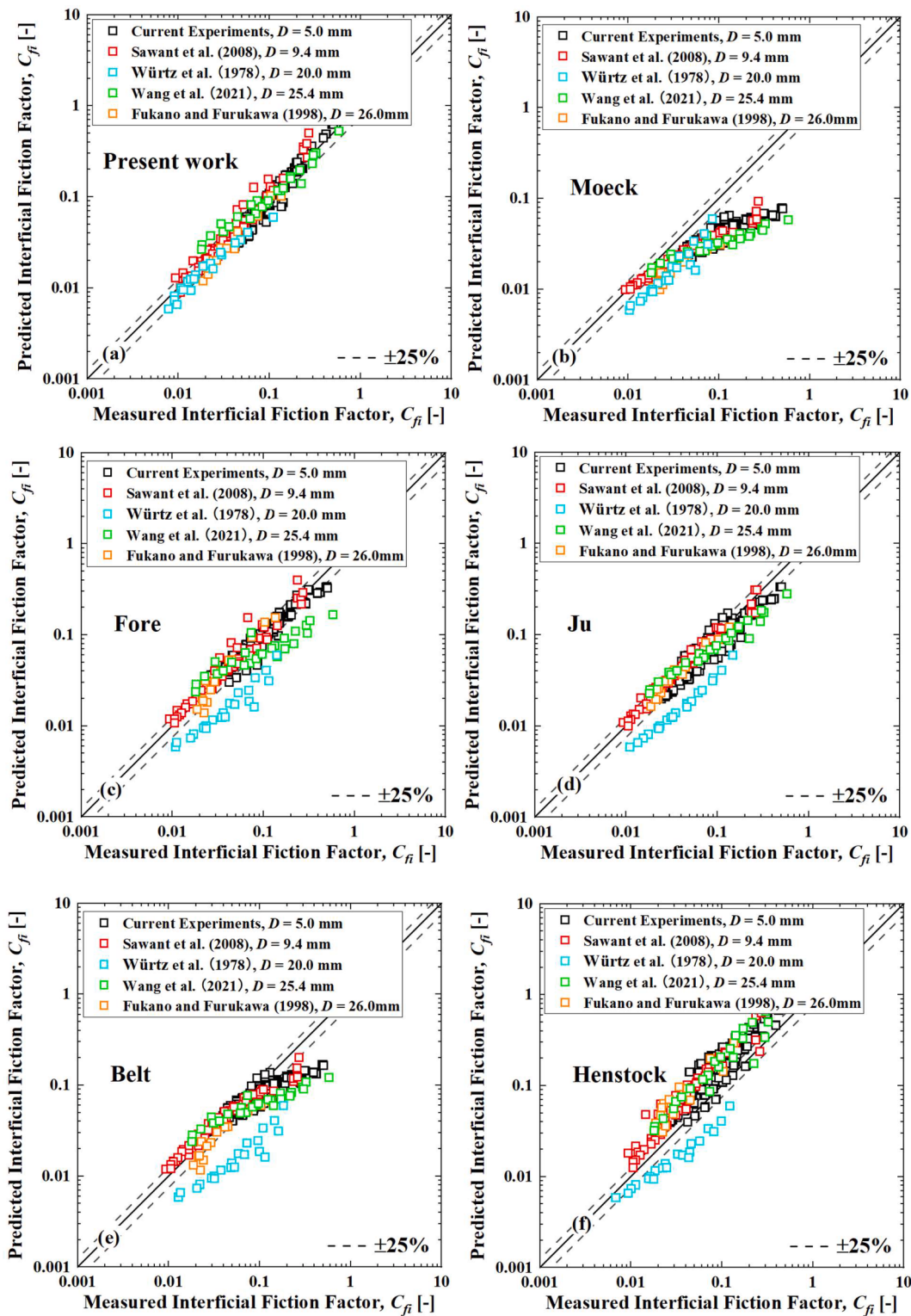


**Fig. 10.** Comparison of the measured and predicted interfacial friction factor from the correlations of the (a) present work, (b) Moeck [2], (c) Fore et al. [4], (d) Ju et al. [5], (e) Belt et al. [9], and (f) Henstock and Hanratty [10].

When  $j_L$  is 0.4 and 0.8 m/s,  $\tau_i$  decreases as the surface tension decreases.

The measured pressure gradient and interfacial shear stress were plotted against the gas Weber number based on our previous study, which noted the predominant effect of the gas Weber number on the film thickness and disturbance wave height [19]. However, the resulting plot did not achieve a precise data.

### 3.2. Interfacial friction factor

Considering  $t_{fave}$  as negligible compared to the tube diameter and difference between the gas core and liquid film, the following relationship was chosen to calculate the interfacial friction factor in this study for simplicity without introducing errors from the measurement:

**Table 4**

Previous correlations for predicting the two-phase pressure drop.

Reference	Correlation
Homogeneous-Cicchitti et al. [36]	$\mu_{TP} = x\mu_G + (1-x)\mu_L$ .
Homogeneous-Awad and Muzychka. [37]	$\mu_{TP} = \mu_G \frac{2\mu_G + \mu_L - 2(\mu_G - \mu_L)(1-x)}{2\mu_G + \mu_L + (\mu_G - \mu_L)(1-x)}$ .
Sun and Mishima [42]	$C = 26 \left(1 + \frac{Re_L}{1000}\right) \left[1 - e^{\left(\frac{-0.153}{0.27 \times La + 0.8}\right)}\right]$ for $Re_L$ and $Re_G < 2000$ ;
Kim and Mudawar [43]	$\phi_L^2 = 1 + \frac{C}{X^{1.19}} + \frac{1}{X^2}$ , $C = 1.79 \left(\frac{Re_G}{Re_L}\right)^{0.4} \left(\frac{1-x}{x}\right)^{0.5}$ for $Re_L \geq 2000$ or $Re_G \geq 2000$ , where $La = \frac{\left(\frac{\sigma}{g(\rho_L - \rho_G)}\right)^{0.5}}{D}$ .

$$\tau_i = \frac{C_{fi} \rho_G j_G^2}{2}. \quad (5)$$

This typical form of  $C_{fi}$  can easily calculate the interfacial shear stress. Thus, it has been widely adopted in previous studies [4,5,9,13, 27].

Wang et al. [30] and Wang et al. [31] noted the close relationship between the interfacial friction factor and interfacial roughness in an annular flow, which is similar for a single-phase flow, whereby the interfacial roughness is dependent on the disturbance wave height,  $H$ . As the interfacial friction factor is usually related to the Reynolds number, the normalized wave height  $H/D$  and interfacial friction factor were plotted against the gas Reynolds number for comparison, as shown in Fig. 5. The liquid and gas Reynolds number are expressed as:

$$Re_{L(G)} = \frac{\rho_{L(G)} j_{L(G)} D}{\mu_{L(G)}}. \quad (6)$$

The wave height is defined as the difference between the base film thickness  $t_{fbase}$  and maximum film thickness  $t_{fmax}$ , as shown in Fig. 6. More detailed information about  $t_{fbase}$  and  $t_{fmax}$  is provided in our previous studies [19,20].

Similar with the findings of Wang et al. [30], both interfacial friction factor and disturbance wave height decrease with the increase in  $Re_G$  under the same liquid flow rate, density ratio, and surface tension. The decrease in the interfacial friction factor is usually accompanied by the decrease in the normalized wave height under the same condition, indicating that the interfacial friction factor is closely related to the disturbance wave height. However, the physical explanation for this phenomenon is still missing.

In a single-phase pipe flow, a Moody chart [32] is widely accepted as a standard approach to estimate the single-phase friction factor using  $Re_G$  and equivalent sand-grain roughness  $k_s$ . Here,  $k_s$  is introduced by Moody [32] to specifically characterize the wall roughness that affect the friction factor. In the Moody chart, the friction factor for a turbulent flow is determined by an approximation introduced by Colebrook [7] based on the measurements of pipe flows with walls covered by real sand by Nikuradse [33]. The Colebrook equation was later modified by simpler equations by Churchill [8]. From Belt et al. [9], the interfacial roughness in an annular flow is analogous to the wall roughness in a single-phase pipe flow. The equivalent sand-grain roughness of the annular flow can be computed by the Churchill equations [8] with the measured interfacial shear stress in annular flow experiments. The equivalent sand-grain roughness of an annular flow is proportional to the wave height, instead of quadruple the mean film thickness as assumed by Wallis et al. [1]. However, the authors did not show the relationship between the sand-grain roughness and disturbance wave height. Instead, a  $C_{fi}$  correlation is proposed based on the linear dependency between the interfacial friction factor and average film

thickness rather than wave height.

As described in [9,17], the normalized equivalent sand-grain roughness  $k_s/D$  can be obtained from the Churchill equation. The Churchill equation employed in this work is expressed as [8]:

$$\frac{1}{\sqrt{C_{fi}}} = 2.457 \ln \left[ \frac{1}{\left(\frac{7}{Re_G}\right)^{0.9} + 0.27 \frac{k_s}{D}} \right]. \quad (7)$$

Through Eq. (7),  $k_s/D$  can be calculated from the measured  $C_{fi}$  in our experiments. The comparison between  $k_s/D$  and  $H/D$  and  $t_{fave}/D$  is presented in Fig. 7. Based on current experimental data, the relationships between  $k_s/D$

$$\frac{k_s}{D} = 18 \frac{H}{D} \quad (8)$$

$$\frac{k_s}{D} = 29 \frac{t_{fave}}{D} \quad (9)$$

For most of our data, a single unifying relationship between  $k_s/D$  and  $H/D$  and  $t_{fave}/D$  exist even under different experimental conditions and flow rates of the working liquid and gas. However, when plotted against  $H/D$ ,  $k_s/D$  is more precise, and the deviation is smaller than that of  $t_{fave}/D$ , as indicated by the 25 % error bar.

As shown in Fig. 8, a single unifying relationship exists between the  $C_{fi}$  and  $H/D$  rather than  $t_{fave}/D$ . This indicates that, even for the annular flow, the equivalent sand-grain roughness which is characterized by the disturbance wave height, is a key factor for the interfacial friction factor in a single-phase turbulent flow, which is described by the famous Moody chart [32]. This could also be extended to explain that the pressure drop and decrease in the interfacial shear stress when surface tension is reduced. As shown in Fig. 5, when the surface tension decreases, the wave height also decreases under the same liquid and gas flow rate and density ratio. Subsequently, the interfacial roughness, as characterized by the wave height, is reduced owing the decrease in the interfacial shear stress.

To predict the interfacial friction factor for an annular flow, we propose a simplified correlation based on the Churchill equation (Eq. (7)). However, Eq. (7) is still complicated and the equivalent sand-grain roughness that comprises the disturbance wave height cannot be easily obtained in practical applications. Thus, the term  $\frac{1}{\left(\frac{7}{Re_G}\right)^{0.9} + 0.27 \frac{k_s}{D}}$  in Eq. (7)

is reduced to a function of a dimensionless number group consisting of the gas Reynolds number, liquid Weber number, and gas Weber number, considering that  $k_s/D$  is related to  $H/D$ , which is a function of the liquid and gas Weber number based on our previous study [19], as shown in Fig. 9. Here, the liquid Weber number and gas Weber number are expressed by:

- Current Experiments,  $D = 5.0$  mm,  $P = 0.2, 0.4$ , and  $0.7$  MPa
- Würtz et al. (1978),  $D = 10.0$  mm,  $P = 7.0$  MPa, Steam-Water system
- Würtz et al. (1978),  $D = 20.0$  mm,  $P = 7.0$  MPa, Steam-Water system
- Wang et al. (2021),  $D = 25.4$  mm,  $P = 0.1$  MPa, Air-water system

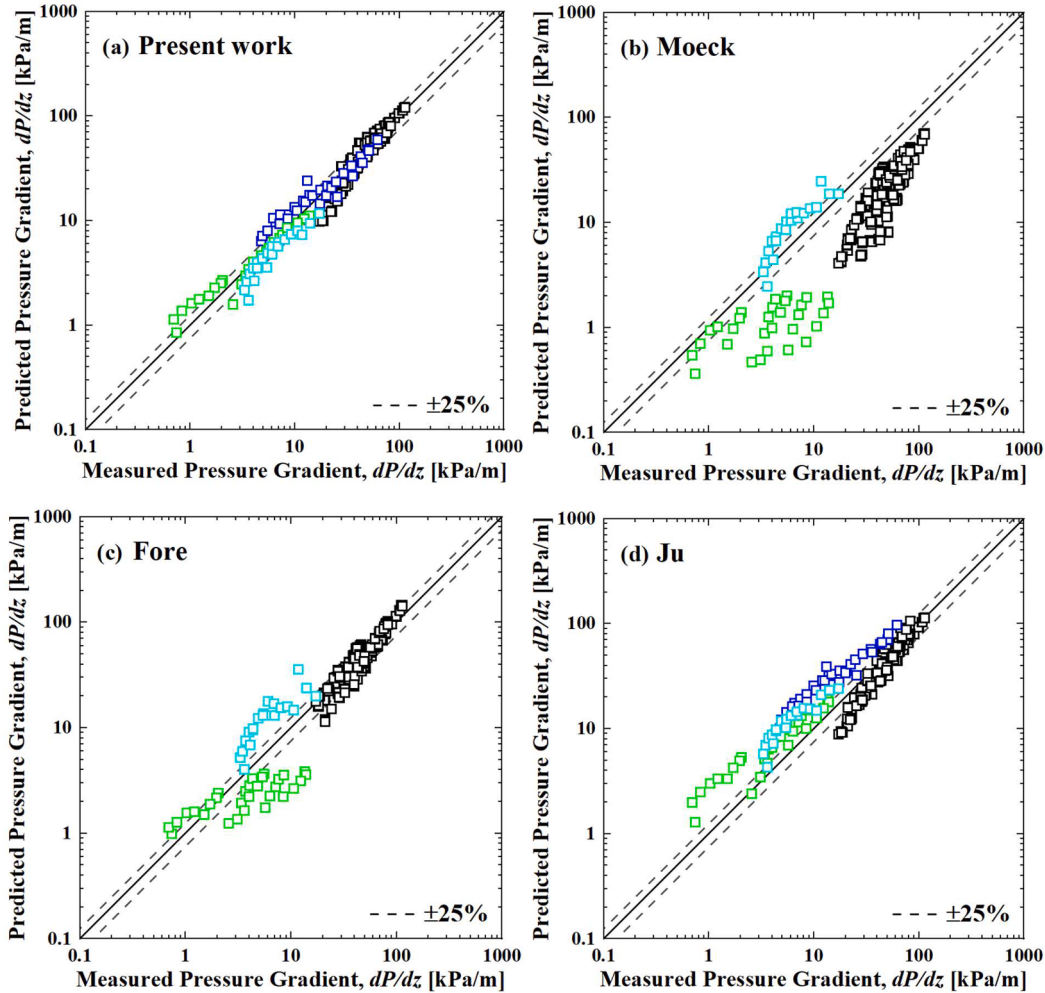


**Fig. 11.** Comparison of the measured and predicted pressure drop by combining Eqs. (4), (5), (23), and  $C_{fi}$  correlations of the (a) present work, (b) Moeck [2], (c) Fore et al. [4], (d) Ju et al. [5], (e) Belt et al. [9], (f) Henstock and Hanratty [10], (g) Cicchitti [36], (h) Awad and Muzychka [37], (i) Sun and Mishima [42], and (j) Kim and Mudwar [43].

$$We_L = \frac{\rho_L j_L^2 D}{\sigma}, \quad (10)$$

$$We_G = \frac{\rho_G j_G^2 D}{\sigma}. \quad (11)$$

Eq. (7) can then be simplified as the following form coefficients A–F:

$$\frac{1}{\sqrt{C_{fi}}} = A \ln[B + C Re_G^D We_L^E We_G^F]. \quad (12)$$

After employing current experimental data and previous databases by Fukano and Furukawa [3], Sawant et al. [34], and Wang et al. [27] (summarized in Table 2) to include the effect of the tube diameter, a new model is derived by multiple regression of Eq. (12):

$$\frac{1}{\sqrt{C_{fi}}} = 8.1 \ln[1.1 + 0.08 Re_G^{0.11} We_L^{-0.24} We_G^{0.52}]. \quad (13)$$

The newly proposed model in this work (Eq. (13)) is evaluated using the current and previous databases and several existing correlations on  $C_{fi}$ , as summarized in Table 3. The comparison between the measured and predicted  $C_{fi}$  is presented in Fig. 10. The correlation from the present work can provide the best prediction performance with an error of ca. 25 % even for the steam–water annular flow under 286 °C and 7 MPa, which is similar to the experimental condition in the boiling water reactors (BWRs) by Würtz [35]. It is worth noting that current model is proposed based on the experimental databases with surface tension ranging from 30.7 to 73.0 mN/m. Even the model could predict the data with surface tension as low as 17.7 mN/m with good performance, more experiments with surface tension lower than 17.7 mN/m are encouraged to examine the model.

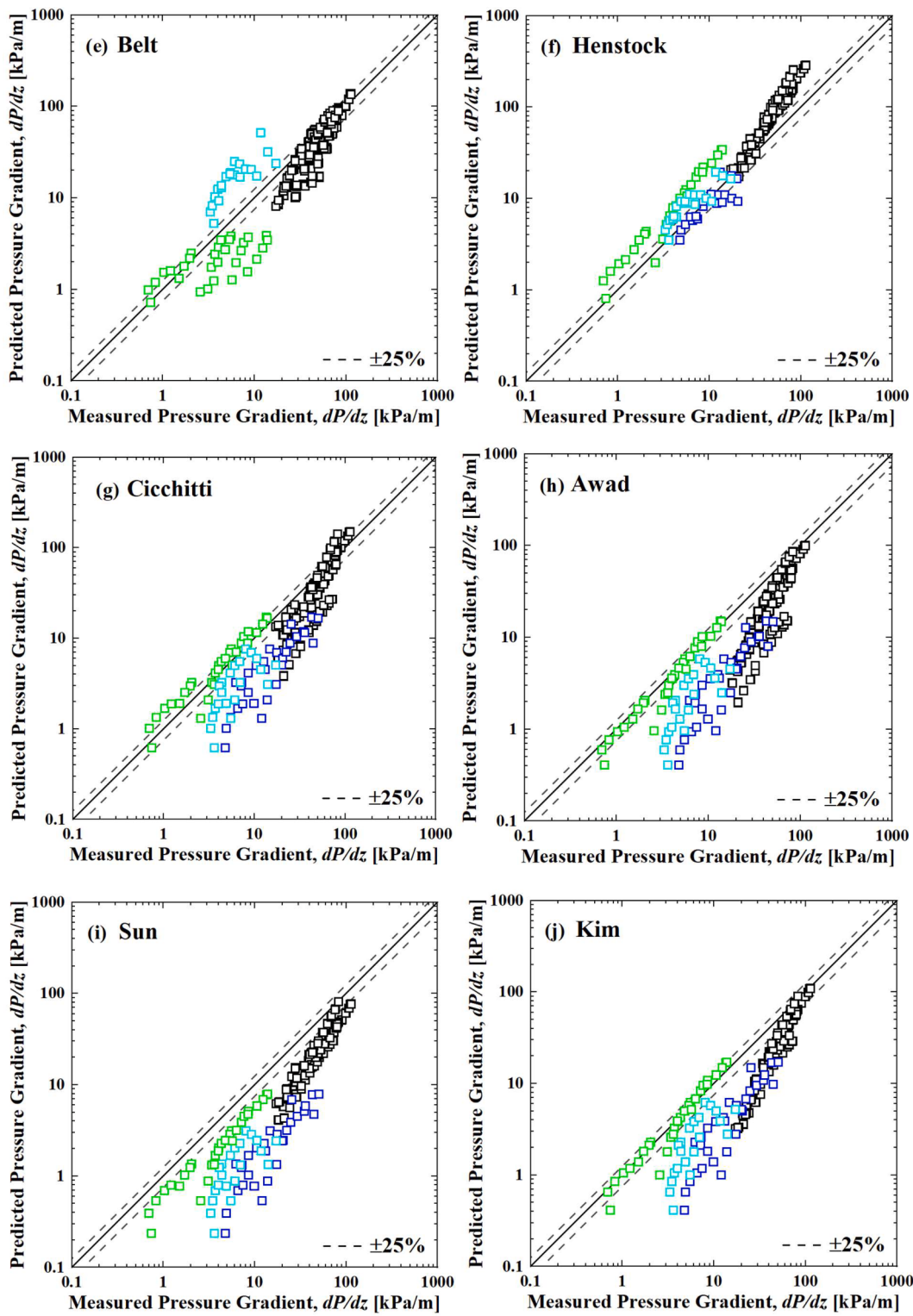


Fig. 11. (continued).

### 3.3. Pressure drop prediction

Conventionally, the frictional pressure drop of a gas–liquid annular flow, is predicted by homogeneous, and separated flow models. In the homogeneous flow model, the liquid, and gas phases are assumed as a mixed single-phase flow with the same velocity. The density of the two-phase homogeneous flow is expressed as:

$$\rho_{TP} = \frac{1}{\left(\frac{x}{\rho_G} + \frac{1-x}{\rho_L}\right)} \quad (14)$$

Where  $x$  is the vapor quality. Subsequently, the frictional pressure gradient of the two-phase homogeneous flow model is given as:

$$-\left(\frac{dP}{dz}\right)_{TP} = \frac{2C_{FTP}G^2}{D\rho_{TP}} \quad (15)$$

Where  $G$  is the mass flux, and  $C_{FTP}$  is the friction factor of the two-phase homogeneous flow, which is expressed as:

$$C_{FTP(L,G)} = \begin{cases} 16/Re_{TP(L,G)}, & Re_{TP(L,G)} < 2000 \\ 0.079Re_{TP(L,G)}^{-0.25}, & 2000 \leq Re_{TP(L,G)} < 20000 \\ 0.046Re_{TP(L,G)}^{-0.2}, & Re_{TP(L,G)} \geq 20000 \end{cases} \quad (16)$$

$$Re_{TP} = \frac{GD}{\mu_{TP}} \quad (17)$$

To calculate the friction factor, the two-phase homogeneous viscosity,  $\mu_{TP}$ , should be determined appropriately to obtain the two-phase Reynolds number ( $Re_{TP}$ ). In this work, two typical correlations for  $\mu_{TP}$  [36,37] with relatively good predictive performance as evaluated by previous researchers [38,39], were chosen for comparison as summarized in the Table 4.

For the separated flow model, the Lockhart–Martinelli method [40] is usually employed to predict the two-phase pressure drop. In this method, the two-phase pressure gradient can be obtained by a single-phase flow pressure gradient of the liquid phase  $(\frac{dP}{dz})_L$  and two-phase frictional multiplier of the liquid phase  $\phi_L$  as

$$\left(\frac{dP}{dz}\right)_{TP} = \phi_L^2 \left(\frac{dP}{dz}\right)_L \quad (18)$$

The correlation by Chisholm [41] is employed to calculate the two-phase frictional multiplier as

$$\phi_L^2 = 1 + \frac{C}{X} + \frac{1}{X^2} \quad (19)$$

where  $C$  is the Chisholm parameter to characterize the interaction effect between the phases, and  $X$  is the Lockhart–Martinelli parameter defined as

$$X^2 = \left(\frac{dP}{dz}\right)_L / \left(\frac{dP}{dz}\right)_G \quad (20)$$

$$-\left(\frac{dP}{dz}\right)_{L(G)} = \frac{2C_{fL(G)}\rho_{L(G)}j_{L(G)}^2}{D} \quad (21)$$

Here, the single-phase friction factor of the liquid and gas phase is obtained by Eq. (18) with the single-phase Reynolds number defined in Eq. (6). Similarly, two correlations of  $C$  with good predictive performance by Sun and Mishima [42] and Kim and Mudawar [43] were employed for the comparison, as summarized in Table 4.

In this work, a new model for predicting the pressure drop was derived. From our previous work [19], the average film thickness can be expressed as:

$$\frac{t_{Fave}}{D} = 0.28Re_L^{-0.14}We_L^{0.25}We_G^{-0.36} \quad (22)$$

Substituting Eqs. (5), (13) and (22) into Eq. (4), the pressure gradient  $dP/dz$  can be roughly predicted by the following equation considering frictional pressure drop as the dominant component of the total pressure drop:

$$\frac{dp}{dz} = -\frac{2\rho_G j_G^2}{D(1 - 0.56Re_L^{-0.14}We_L^{0.25}We_G^{-0.36})(8.1\ln[1.1 + 0.08Re_G^{0.11}We_L^{-0.24}We_G^{0.52}])^2} \quad (23)$$

Fig. 11 shows a comparison of Eq. (23), Eq. (23) with the term  $(8.1\ln[1.1 + 0.08Re_G^{0.11}We_L^{-0.24}We_G^{0.52}])^2$  replaced by other  $C_{fi}$  correlations listed in Table 3, and homogeneous, and separated flow models listed in Table 4 employing the databases of Wang et al. [27] and Würzt

[35]. As the database of Würzt [35] in the 10.0-mm (inner diameter) tube did not provide information on the average film thickness, it was included in the comparison using the  $C_{fi}$  correlations by Moeck [2], Fore et al. [4], and Belt et al. [9]. It is readily apparent that the correlations of the homogeneous and separated flow models could provide good predictions for the experimental data by Wang et al. However, the deviation increases using the datasets by Würzt, which correspond to the steam–water annular flow under 7 MPa and 286 °C. Among the other models, our model exhibited the best predictive performance with an error of approximately 25 % for different fluids properties.

#### 4. Conclusion

Based on the upward annular flow experimental of nitrogen–water, HFC134a–water, and nitrogen–95% ethanol solution, a theoretical analysis on the interfacial shear stress was performed. Models were developed to predict the interfacial shear stress and pressure drop for the upward annular flow. The main conclusions are as follows:

- (1) Based on the present experimental results, the interfacial shear stress increased with the decrease in the density ratio and decreased with the decrease in the surface tension, which could be attributed to the reduced interfacial roughness characterized by the disturbance wave height.
- (2) From the current experimental data, the equivalent sand-grain roughness, as employed in the Moody chart, was directly related with the wave height for the annular flow. A correlation (Eq. (13)) was proposed in the form of the Churchill equation to predict the interfacial friction factor with relatively good predictive performance.
- (3) A model (Eq. (23)) was proposed to predict the pressure drop for an upward annular flow. It was compared with previous models using existing databases, including steam–water annular flow under similar conditions that of a BWR, whereby a good prediction accuracy was demonstrated.

#### CRediT authorship contribution statement

**Huacheng Zhang:** Investigation, Conceptualization, Data curation, Writing – original draft, Writing – review & editing. **Yutaro Umehara:** Investigation, Conceptualization, Writing – original draft. **Hiroyuki Yoshida:** Investigation, Conceptualization, Funding acquisition. **Shojo Mori:** Investigation, Conceptualization, Data curation, Writing – original draft, Writing – review & editing, Supervision.

#### Declaration of Competing Interest

The authors declare that they have no known competing financial interests or personal relationships that could have appeared to influence the work reported in this paper.

#### Data availability

Data will be made available on request.

#### References

- [1] G.B. Wallis, One-Dimensional Two-Phase Flow, McGraw-Hill, New York, 1969.
- [2] E.O. Moeck, Annular-Dispersed Two-Phase Flow and Critical Heat Flux, AECL, 1970, p. 3656.
- [3] T. Fukano, T. Furukawa, Prediction of the effects of liquid viscosity on interfacial shear stress and frictional pressure drop in vertical upward gas–liquid annular flow, Int. J. Multiph. Flow. 24 (1998) 587–603, [https://doi.org/10.1016/S0301-9322\(97\)00070-0](https://doi.org/10.1016/S0301-9322(97)00070-0).
- [4] L.B. Fore, S.G. Beus, R.C. Bauer, Interfacial friction in gas–liquid annular flow: analogies to full and transition roughness, Int. J. Multiph. Flow. 26 (2000) 1755–1769, [https://doi.org/10.1016/S0301-9322\(99\)00114-7](https://doi.org/10.1016/S0301-9322(99)00114-7).

- [5] P. Ju, Y. Liu, C.S. Brooks, M. Ishii, Prediction of interfacial shear stress of vertical upward adiabatic annular flow in pipes, *Int. J. Heat Mass Transf.* 133 (2019) 500–509, <https://doi.org/10.1016/j.ijheatmasstransfer.2018.12.057>.
- [6] R.V.A. Oliemans, B.F.M. Pots, N. Trompé, Modelling of annular dispersed two-phase flow in vertical pipes, *Int. J. Multiph. Flow.* 12 (1986) 711–732, [https://doi.org/10.1016/0301-9322\(86\)90047-9](https://doi.org/10.1016/0301-9322(86)90047-9).
- [7] C.F. Colebrook, Turbulent flow in pipes, with particular reference to the transition region between the smooth and rough pipe laws, *J. Inst. Civ. Eng.* 11 (1939) 133–156, <https://doi.org/10.1680/ijoti.1939.14509>.
- [8] S.W. Churchill, Friction-factor equation spans all fluid-flow regimes, *Chem. Eng.* 84 (1977) 91–92.
- [9] R.J. Belt, J.M.C. Van't Westende, L.M. Portela, Prediction of the interfacial shear-stress in vertical annular flow, *Int. J. Multiph. Flow.* 35 (2009) 689–697, <https://doi.org/10.1016/j.ijmultiphaseflow.2008.12.003>.
- [10] W.H. Henstock, T.J. Hanratty, The interfacial drag and the height of the wall layer in annular flows, *AIChE J.* 22 (1976) 990–1000, <https://doi.org/10.1002/aic.690220607>.
- [11] J.C. Asali, T.J. Hanratty, P. Andreussi, Interfacial drag and film height for vertical annular flow, *AIChE J.* 31 (1985) 895–902, <https://doi.org/10.1002/aic.690310604>.
- [12] M. Hajiloo, B.H. Chang, A.F. Mills, Interfacial shear in downward two-phase annular co-current flow, *Int. J. Multiph. Flow.* 27 (2001) 1095–1108, [https://doi.org/10.1016/S0301-9322\(00\)00065-3](https://doi.org/10.1016/S0301-9322(00)00065-3).
- [13] A.M. Aliyu, L. Lao, A.A. Almabrok, H. Yeung, Interfacial shear in adiabatic downward gas/liquid co-current annular flow in pipes, *Exp. Therm. Fluid Sci.* 72 (2016) 75–87, <https://doi.org/10.1016/j.expthermflusci.2015.10.025>.
- [14] A.M. Aliyu, Y.D. Baba, L. Lao, H. Yeung, K.C. Kim, Interfacial friction in upward annular gas-liquid two-phase flow in pipes, *Exp. Therm. Fluid Sci.* 84 (2017) 90–109, <https://doi.org/10.1016/j.expthermflusci.2017.02.006>.
- [15] A. Cioncolini, J.R. Thome, C. Lombardi, Unified macro-to-micromodel method to predict two-phase frictional pressure drops of annular flows, *Int. J. Multiph. Flow.* 35 (2009) 1138–1148, <https://doi.org/10.1016/j.ijmultiphaseflow.2009.07.005>.
- [16] A. Kawahara, M.H. Mansour, M. Sadatomi, W.Z. Law, H. Kurihara, H. Kusumaningsih, Characteristics of gas-liquid two-phase flows through a sudden contraction in rectangular microchannels, *Exp. Therm. Fluid Sci.* 66 (2015) 243–253, <https://doi.org/10.1016/j.expthermflusci.2015.03.030>.
- [17] T.S. Zhao, Q.C. Bi, Pressure drop characteristics of gas-liquid two-phase flow in vertical miniature triangular channels, *Int. J. Heat Mass Transf.* 44 (2001) 2523–2534, [https://doi.org/10.1016/S0017-9310\(00\)00282-9](https://doi.org/10.1016/S0017-9310(00)00282-9).
- [18] R. Goda, R. Kurimoto, K. Hayashi, M. Murase, A. Tomiyama, Effects of fluid properties on interfacial and wall friction factors under counter-current flow limitation in a vertical pipe with sharp-edged lower end, *Nucl. Eng. Des.* 373 (2021), 111020, <https://doi.org/10.1016/j.nucengdes.2020.111020>.
- [19] H. Zhang, S. Mori, T. Hisano, H. Yoshida, Effect of gas density and surface tension on liquid film thickness in vertical upward disturbance wave flow, *Int. J. Multiph. Flow.* 159 (2023), 104342, <https://doi.org/10.1016/j.ijmultiphaseflow.2022.104342>.
- [20] H. Zhang, Y. Umehara, H. Yoshida, S. Mori, On the velocity and frequency of disturbance waves in vertical annular flow with different surface tension and gas-liquid density ratio, *Int. J. Heat Mass Transf.* 211 (2023), 124253, <https://doi.org/10.1016/j.ijheatmasstransfer.2023.124253>.
- [21] G.F. Hewitt, N.S. Hall-Taylor, *Annular Two-Phase Flow*, 1st Ed., Pergamon Press, Oxford, New York, 1970.
- [22] I. Kataoka, M. Ishii, *Mechanism and Correlation of Droplet Entrainment and Deposition in Annular Two-Phase Flow*, Argonne National Lab., IL (USA), 1982. NUREG/CR-2885.
- [23] N.B. Vargaftik, *Handbook of Physical Properties of Liquids and Gases-Pure Substances and Mixtures*, Hemisphere Publishing Corporation, New, York, 1975.
- [24] G.F. Hewitt, D.N. Roberts, Studies of two-phase flow patterns by simultaneous x-ray and fast photography. No. AERE-M-2159, Atomic Energy Research Establishment, Harwell, England (United Kingdom), 1969.
- [25] K. Mishima, M. Ishii, Flow regime transition criteria for upward two-phase flow in vertical tubes, *Int. J. Heat Mass Transf.* 27 (1984) 723–737, [https://doi.org/10.1016/0017-9310\(84\)90142-X](https://doi.org/10.1016/0017-9310(84)90142-X).
- [26] D. Schubring, T.A. Shedd, E.T. Hurlbut, Planar laser-induced fluorescence (PLIF) measurements of liquid film thickness in annular flow. part II: analysis and comparison to models, *Int. J. Multiph. Flow.* 36 (2010) 825–835, <https://doi.org/10.1016/j.ijmultiphaseflow.2010.02.002>.
- [27] G. Wang, Z. Dang, M. Ishii, Wave structure and velocity in vertical upward annular two-phase flow, *Exp. Therm. Fluid Sci.* 120 (2021), 110205, <https://doi.org/10.1016/j.expthermflusci.2020.110205>.
- [28] P. Sawant, M. Ishii, M. Mori, Droplet entrainment correlation in vertical upward co-current annular two-phase flow, *Nucl. Eng. Des.* 238 (2008) 1342–1352, <https://doi.org/10.1016/j.nucengdes.2007.10.005>.
- [29] M. Ishii, K. Mishima, Correlation for liquid entrainment in annular two-phase flow of low viscous fluid. Argonne National Laboratory Report ANL/RA/LWR 81-2, 1981.
- [30] Z. Wang, K.S. Gabriel, D.L. Manz, The influences of wave height on the interfacial friction in annular gas-liquid flow under normal and microgravity conditions, *Int. J. Multiph. Flow.* 30 (2004) 1193–1211, <https://doi.org/10.1016/j.ijmultiphaseflow.2004.06.003>.
- [31] C. Wang, N. Zhao, Y. Feng, H. Sun, L. Fang, Interfacial wave velocity of vertical gas-liquid annular flow at different system pressures, *Exp. Therm. Fluid Sci.* 92 (2018) 20–32, <https://doi.org/10.1016/j.expthermflusci.2017.09.007>.
- [32] L.F. Moody, Friction factors for pipe flow, *J. Fluids Eng.* 66 (1944) 671–678, <https://doi.org/10.1115/1.4018140>.
- [33] J. Nikuradse, *Strömungsgesetze in rauen Rohren*. VDI-Forschungsheft 361. Beilage zu "Forschung auf dem Gebiete des Ingenieurwesens, Ausgabe B Band 4 (1933).
- [34] P. Sawant, *Dynamics of annular two-phase flow* (Ph.D, Purdue University, West Lafayette, USA, 2008).
- [35] J. Würtz, *An Experimental and Theoretical Investigation of Annular Steam-Water Flow in Tubes and Annuli at 30 to 90 Bar*, Risø National Laboratory Roskilde, 1978.
- [36] A. Cicchitti, C. Lombardi, M. Silvestri, Two-phase cooling experiments: pressure drop, heat transfer and burnout measurements, *Energy Nucl.* 7 (1960) 417–425.
- [37] M.M. Awad, Y.S. Muzychka, Effective property models for homogeneous two-phase flows, *Exp. Therm. Fluid Sci.* 33 (2008) 106–113, <https://doi.org/10.1016/j.expthermflusci.2008.07.006>.
- [38] H. Li, P. Hrnjak, Heat transfer coefficient, pressure gradient, and flow patterns of R1233zd(E) and R1336mzz(Z) evaporating in a microchannel tube, *Int. J. Heat Mass Transf.* 182 (2022), 121992, <https://doi.org/10.1016/j.ijheatmasstransfer.2021.121992>.
- [39] F. Nie, S. Yan, H. Wang, C. Zhao, Y. Zhao, M. Gong, A universal correlation for predicting two-phase frictional pressure drop in horizontal tubes based on machine learning, *Int. J. Multiph. Flow.* 160 (2023), 104377, <https://doi.org/10.1016/j.ijmultiphaseflow.2022.104377>.
- [40] W. Lockhart, R.C. Martinelli, Proposed correlation of data for isothermal two-phase, two-component flow in pipes, *Chem. Eng. Prog.* 45 (1949) 39–48.
- [41] D. Chisholm, Pressure gradients due to friction during the flow of evaporating two-phase mixtures in smooth tubes and channels, *Int. J. Heat Mass Transf.* 16 (1973) 347–358, [https://doi.org/10.1016/0017-9310\(73\)90063-X](https://doi.org/10.1016/0017-9310(73)90063-X).
- [42] L. Sun, K. Mishima, Evaluation analysis of prediction methods for two-phase flow pressure drop in mini-channels, *Int. J. Multiph. Flow.* (2009), <https://doi.org/10.1016/j.ijmultiphaseflow.2008.08.003>.
- [43] S.M. Kim, I. Mudawar, Universal approach to predicting two-phase frictional pressure drop for adiabatic and condensing mini/micro-channel flows, *Int. J. Heat Mass Transf.* 55 (2012) 3246–3261, <https://doi.org/10.1016/j.ijheatmasstransfer.2012.02.047>.